Seismic performance of exoskeleton structures

Anna Reggio, Luciana Restuccia, Lucrezia Martelli, Giuseppe Andrea Ferro

HIGHLIGHTS

- Performance of exoskeleton structures as structural control systems under seismic loading
- Rigid coupling between the primary structure and the exoskeleton structure
- The dynamic behaviour of the coupled system is characterised in frequency domain
- RC frame connected to steel diagrid-like exoskeleton structure discussed as case study
- Displacement, deformation and internal force control obtained for the primary structure

Seismic performance of exoskeleton structures

Anna Reggio[a,*], Luciana Restuccia[a], Lucrezia Martelli[a], Giuseppe Andrea Ferro[a]

[a]*Department of Structural, Geotechnical and Building Engineering, Politecnico di Torino, Corso Duca degli Abruzzi 24, 10129 Torino, Italy*

Abstract

Biomimetic exoskeleton structures are external self-supporting structural systems suitably connected to primary inner structures, the latter being enhanced or protected, in a general sense, by virtue of this connection. Their potential asset for an integrated retrofitting approach, combining structural safety and sustainability merit, has recently drawn considerable attention. In this work, the focus is on investigating the performance of exoskeleton structures as structural control systems under seismic loading. The exoskeleton structure is modelled as a dynamic system whose mass (in principle, not negligible), stiffness and damping properties can be varied and, possibly, designed with the aim of controlling the response of the primary structure. A non-dissipative, and in particular rigid, coupling is assumed between the primary structure and the exoskeleton structure. A first insight into the dynamic behaviour of the coupled system is gained in frequency domain. The dynamic equilibrium is set in non-dimensional form and the response to harmonic base motion is analysed with varying system parameters. Complex-valued Frequency Response Functions are used as performance evaluators in terms of relative displacement, absolute acceleration and transmitted force. A case study is subsequently discussed, dealing with the seismic response of a mid-rise reinforced concrete frame, designed with non-ductile behaviour, coupled to a steel diagrid-like lattice exoskeleton structure. Results of the seismic analyses show that the rigid coupling to the exoskeleton

*Corresponding author.
Email address: anna.reggio@polito.it (Anna Reggio)

structure allows to achieve a significant displacement and deformation control of the primary structure, as well as important reductions of its internal forces, in terms of both base and floor shear forces.
Keywords: structural dynamics, structural control, exoskeleton structure, coupling, base motion, frequency response, seismic response

1. Introduction

Endowed with biomimetic meaning, the locution *exoskeleton structure* is used to indicate a self-supporting structural system set outside and suitably connected to a primary inner structure, the latter being enhanced or protected, in a general sense, by virtue of this connection. Attention has been recently drawn to the potential asset of exoskeleton structures for an integrated retrofitting approach of existing buildings, in which structural safety as well as energy efficiency, environmental sustainability and architectural quality are improved in a combined and coordinated way [1, 2, 3].

In earthquake-prone regions, where innovative structural control systems are crucial to the achievement of a resilient built environment [4, 5, 6, 7], the feasibility of exoskeleton structures for seismic protection is particularly worthy of being investigated [8]. In the present study, the exoskeleton structure is hence regarded as a structural control system that can be designed for the external seismic retrofitting of a building frame structure. External structural control systems, like reinforced concrete cores and walls [9, 10, 11], stepping and pinned rocking walls [12, 13, 14] and reaction towers [15, 16, 17, 18], are considered in literature as a promising strategy due to a number of reasons: service or business downtime as well as residents displacement are kept to a minimum, because the retrofitting process is operated from outside of the building; interference with existing structural and nonstructural components is limited; the possible strengthening of structural members is restricted to the ones locally interested by the connections to the external control system. Exoskeleton structures further meet a number of advantages specific to them: they can boost

both the economical and the ecological efficiency of the retrofitting intervention, thanks to the above-mentioned potential for a multifunctional integrated design; depending on urban planning restrictions, they may either adhere to or be an expansion of the existing building, thereby allowing for additional housing spaces and increased real estate value; they foster the building technological updating and the urban regeneration [19, 20].

The aim of the present study is to explore the seismic performance of exoskeleton structures and their ability to reduce the earthquake-induced vibrations of existing frame structures. The consideration of an *intra*-connection between two subsystems of a same, single structural system is a distinctive aspect of this study and, compared to previous literature about the *inter*-connection between adjacent structures, it involves essential differences that have to be highlighted.

Most literature works on adjacent structures focus on buildings with given dynamic properties, subsequently coupled at storey level to limit structural damage or avoid pounding under dynamic loading. The coupling is electively dissipative, implementing viscous [21, 22, 23], visco-elastic [24, 25, 26, 27] or hysteretic [28, 29, 30, 31] dampers, aimed at providing supplemental energy dissipation. A relative motion between the two structures is therefore essential and ensured by substantially different dynamic properties. The main issue discussed by these work is the design of the dissipative coupling [32, 33], generally optimised according to a global protection strategy, so that the overall response of both the coupled structures is reduced [11].

In this paper, the exoskeleton structure is conceived as a "sacrificial appendage", called to absorb seismic loads in order to increase the performance of a primary frame structure. A non-dissipative, and in particular rigid, coupling is assumed between the primary structure and the exoskeleton structure. The focus is on investigating how such a rigid coupling affects the dynamic response of the primary structure and whether it could be useful for vibration control objectives under seismic loading. The approach of study is the most general one. Given that, in principle, the mass of the exoskeleton structure is not neg-

ligible, dynamic coupling is fully taken into account. The exoskeleton structure is modelled as a dynamic system whose properties, in terms of mass, stiffness and damping, can be varied and, possibly, designed with the aim of controlling the response of the primary structure.

The paper is arranged as follows. After the Introduction, the dynamic model of the system composed of two coupled linear viscoelastic oscillators is defined in Section 2: such a model is of interest, first, due to its paradigmatic value, and second, because it has been proved to be representative of the reduced-order modal model of coupled multi-degree-of-freedom structures [25]. The dynamic equilibrium of the coupled system is set in non-dimensional form, identifying the governing independent parameters, and a parametric study is carried out in frequency domain on the response to harmonic base motion. The results, discussed in Section 3, lead to characterise the dynamic behaviour of the coupled system and to discern the principle of operation delineated by the exoskeleton structure in terms of vibration control. A case study is subsequently presented in Section 4, dealing with the seismic response of a mid-rise reinforced concrete frame structure, designed with non-ductile behaviour, coupled to a steel diagrid-like lattice exoskeleton structure. This choice was motivated by the consideration that diagrid systems are a structural typology particularly appealing for exoskeleton structures, thanks to their inherent structural efficiency, morphological versatility and architectural quality [34], as well as for the possible standardisation and replicability of components [35]. Conclusions are finally drawn in Section 5.

2. Structural model

Without lack of generality, the system composed of a primary structure connected to an exoskeleton structure is modelled by means of two coupled linear viscoelastic oscillators (Figure 1). The primary oscillator, with M_1, K_1 and C_1 as mass, stiffness and damping coefficients, represents the primary structure; the secondary oscillator, with M_2, K_2 and C_2 as mass, stiffness and damping coeffi-

cients, represents the exoskeleton structure; coupling between the two oscillators is assumed to be non-dissipative and is modelled as a Hooke spring with stiffness coefficient K. When the system is excited by a base motion $X_{\mathrm{g}}(t)$, the dynamic equilibrium is written with reference to relative displacements $U_1 = X_1 - X_{\mathrm{g}}$ and $U_2 = X_2 - X_{\mathrm{g}}$ as

$$M_1 U_1'' + C_1 U_1' + K_1 U_1 = -M_1 X_{\mathrm{g}}'' + K(U_2 - U_1) \tag{1a}$$

$$M_2 U_2'' + C_2 U_2' + K_2 U_2 = -M_2 X_{\mathrm{g}}'' - K(U_2 - U_1), \tag{1b}$$

with $(\cdot)'$ denoting differentiation with respect to time t.

The limit case of the Hooke spring with the stiffness coefficient tending to infinity, $K \to \infty$, can be viewed as the case of a rigid coupling between primary and secondary oscillator. It follows $U_2 \to U_1$ and, to the limit, Equations 1 are replaced by the equation of motion of a single-degree-of-freedom (sdof) system:

$$(M_1 + M_2) U_1'' + (C_1 + C_2) U_1' + (K_1 + K_2) U_1 = -(M_1 + M_2) X_{\mathrm{g}}''. \tag{2}$$

To give a more general description of the problem, Equation 2 is rendered non-dimensional by scaling with respect to the chosen characteristic values of frequency $\Omega_1 = \sqrt{K_1/M_1}$, displacement $U^* = M_1 g/K_1$ and force $F^* = M_1 g$, being Ω_1 the uncoupled natural frequency of the primary oscillator and g the acceleration due to gravity. Dimensionless variables $\tau = \Omega_1 t$ and $u_1 = U_1/U^*$ are thus defined and Equation 2 is set in non-dimensional form as

$$(1+\mu)\ddot{u}_1 + (2\zeta_1 + 2\zeta_2 \alpha \mu)\dot{u}_1 + (1 + \alpha^2 \mu) u_1 = -(1+\mu)\ddot{x}_{\mathrm{g}}, \tag{3}$$

with the overdot indicating differentiation with respect to dimensionless time τ. Relevant independent parameters in (3) are:

$$\mu = \frac{M_2}{M_1}, \qquad \alpha = \frac{\Omega_2}{\Omega_1}, \qquad \zeta_1 = \frac{C_1}{2\sqrt{K_1 M_1}}, \qquad \zeta_2 = \frac{C_2}{2\sqrt{K_2 M_2}}. \tag{4}$$

The mass ratio and the frequency ratio between the two oscillators are denoted by μ and α, respectively, with Ω_2 being the uncoupled natural frequency of the secondary oscillator; ζ_1 and ζ_2 are the uncoupled damping ratios of the primary and of the secondary oscillator; non-dimensional base acceleration $\ddot{x}_{\mathrm{g}}$ results to be scaled by gravity.

3. Frequency response

We characterise the dynamic behaviour of the coupled primary-secondary oscillator system in frequency domain, a representation that is natural and effective when dealing with the performance of structural control strategies [36, 37, 38]. Complex-valued Frequency Response Functions (FRFs) are defined and used as performance evaluators for each one of the response quantities of interest: displacement u_1 relative to the base and absolute acceleration $\ddot{x}_1$ of the coupled system; force f transmitted from the moving base to the mass of the coupled system.

3.1. Displacement and acceleration response

Motion $x_{\mathrm{g}}(\tau)$ of the base and steady-state relative displacement response $u_1(\tau)$ of the coupled system are assumed to be harmonic with the same non-dimensional circular frequency $\omega = \Omega/\Omega_1$. They are represented in the form of rotating vectors in Gauss-Argand plane:

$$x_{\mathrm{g}}(\tau) = x_{\mathrm{g}0}\mathrm{e}^{i\omega\tau}, \qquad u_1(\tau) = u_{10}\mathrm{e}^{i\omega\tau}, \tag{5}$$

with $x_{\mathrm{g}0}$ and u_{10} being complex amplitudes with different phasing. By introducing the harmonic functions (5) into the equation of motion (3), we derive the following FRFs:

$$H_{u_1\ddot{x}_{\mathrm{g}}}(\omega) = \frac{u_{10}}{\ddot{x}_{\mathrm{g}0}} = -\frac{1+\mu}{1+\alpha^2\mu + \mathrm{i}\omega(2\zeta_1 + 2\zeta_2\alpha\mu) - \omega^2(1+\mu)}, \tag{6}$$

giving the ratio between the amplitude u_{10} of the system relative displacement and the amplitude $\ddot{x}_{\mathrm{g}0}$ of base acceleration, and

$$H_{\ddot{x}_1\ddot{x}_{\mathrm{g}}}(\omega) = \frac{\ddot{x}_{10}}{\ddot{x}_{\mathrm{g}0}} = \frac{1+\alpha^2\mu + \mathrm{i}\omega(2\zeta_1 + 2\zeta_2\alpha\mu)}{1+\alpha^2\mu + \mathrm{i}\omega(2\zeta_1 + 2\zeta_2\alpha\mu) - \omega^2(1+\mu)}, \tag{7}$$

giving the ratio between the amplitude $\ddot{x}_{10} = \ddot{u}_{10} + \ddot{x}_{\mathrm{g}0}$ of the system absolute acceleration and the amplitude $\ddot{x}_{\mathrm{g}0}$ of base acceleration.

In Figure 2, the magnitude of both FRFs (6) and (7) is plotted versus the excitation frequency ω; for comparison purposes, the corresponding FRFs of the

uncoupled primary oscillator are shown as well. Within the set of parameters (4) governing the dynamic behaviour of the coupled system, $\mu = 0.05$, $\zeta_1 = 0.05$ and $\zeta_2 = 0.05$ are fixed, while frequency ratio α is varied in the range [0.1, 10]: increments of frequency ratio α, for a constant mass ratio μ, correspond to the stiffening of the secondary oscillator with respect to the primary oscillator. As α increases, the FRFs peak, which denotes the resonance frequency of the coupled system, is progressively shifted towards higher frequency values. A second observation is that, while the peak magnitude considerably decreases for the relative displacement FRF (6) , it slightly increases for the absolute acceleration FRF (7).

In consideration of the above results, parametric analyses are carried out to thoroughly explore the dynamic response of the coupled system. Two response ratios are defined in terms of FRF peak magnitude:

$$R_{u_1} = \frac{\max |H_{u_1 \ddot{x}_g}(\omega)|^{\mathrm{C}}}{\max |H_{u_1 \ddot{x}_g}(\omega)|^{\mathrm{U}}}, \qquad R_{\ddot{x}_1} = \frac{\max |H_{\ddot{x}_1 \ddot{x}_g}(\omega)|^{\mathrm{C}}}{\max |H_{\ddot{x}_1 \ddot{x}_g}(\omega)|^{\mathrm{U}}}, \tag{8}$$

where superscripts C and U denote, respectively, the Coupled primary-secondary oscillator system and the Uncoupled primary oscillator. Based on definitions (8), values of R_{u_1} or $R_{\ddot{x}_1}$ smaller than one imply a reduction of the resonance response of the primary oscillator, in terms of relative displacement or absolute acceleration, by virtue of the rigid coupling to the secondary oscillator. Parameters to be studied are mass ratio μ and frequency ratio α, considered as the design parameters of the coupled system. Conversely, damping ratios ζ_1 and ζ_2 are taken as given properties of the oscillators, both equal to 0.05. Results are presented in Figure 3 for μ ranging from 0.001 to 0.20 and α ranging from 0.1 to 20.

Although minima are non found, it appears from Figures 3(a) that R_{u_1} assumes values lower than one in a large part of the spanned parameters space, indicating that the displacement response of the primary oscillator can be significantly reduced by way of the rigid coupling to the secondary oscillator; in particular, $R_{u_1} < 1$ when $\alpha > 1$. Figures 3(b) show, however, that, where the displacement response is reduced, the acceleration response is amplified instead

($R_{\ddot{x}_1} > 1$), a drawback that should be carefully taken into account when dealing with vibration control objectives. It is worth noting that, for $\mu > 0.10$, R_{u_1} appears to be more sensitive to variations in frequency ratio α than in mass ratio μ: it means that, even with a limited mass, but proper dynamic properties, the coupled secondary oscillator is able to effectively control the displacement response of the primary oscillator.

3.2. Transmitted force

A response quantity of interest in the base excitation problem is the force transmitted to the mass of the system due to the motion of the base [39].

From the free-body diagram in Figure 1(b), the force transmitted to the mass of the coupled system is the sum of the forces through the springs and dampers, $F = (K_1 + K_2)U_1 + (C_1 + C_2)U_1'$. By resorting to non-dimensional form and assuming the system harmonic response $u_1(\tau)$ given in (5), it becomes:

$$f(\tau) = (1 + \alpha^2\mu)u_{10}\mathrm{e}^{i\omega\tau} + i\omega(2\zeta_1 + 2\zeta_2\alpha\mu)u_{10}\mathrm{e}^{i\omega\tau} = f_0\mathrm{e}^{i\omega\tau}, \tag{9}$$

where f_0 is the complex amplitude of the transmitted force. We define an FRF giving the ratio between the amplitude of the transmitted force and the amplitude of base acceleration:

$$H_{f\ddot{x}_\mathrm{g}}(\omega) = \frac{f_0}{\ddot{x}_{\mathrm{g}0}} = (1 + \alpha^2\mu + i\omega 2\zeta_1 + i\omega 2\zeta_2\alpha\mu)\, H_{u_1\ddot{x}_\mathrm{g}}(\omega), \tag{10}$$

being $H_{u_1\ddot{x}_\mathrm{g}}(\omega)$ the relative displacement FRF introduced in Equation (6).

Due to the kinematic constraint between the two coupled oscillators, it is possible to split the total transmitted force (9) into the sum of the forces transmitted through each oscillator:

$$f(\tau) = f_1(\tau) + f_2(\tau) = f_{10}\mathrm{e}^{i\omega\tau} + f_{20}\mathrm{e}^{i\omega\tau}. \tag{11}$$

Consequently,

$$H_{f_1\ddot{x}_\mathrm{g}}(\omega) = \frac{f_{01}}{\ddot{x}_{\mathrm{g}0}} = (1 + i\omega 2\zeta_1)\, H_{u_1\ddot{x}_\mathrm{g}}(\omega) \tag{12}$$

and

$$H_{f_2\ddot{x}_\mathrm{g}}(\omega) = \frac{f_{02}}{\ddot{x}_{\mathrm{g}0}} = (\alpha^2\mu + i\omega 2\zeta_2\alpha\mu)\, H_{u_1\ddot{x}_\mathrm{g}}(\omega) \tag{13}$$

are the FRFs measuring the amplitudes f_{10} and f_{20} of the forces transmitted, respectively, through the primary and the secondary oscillator, per unit base acceleration.

Comparisons concerning transmitted forces are drawn in Figure 4. As in Figure 2, parameters $\mu = 0.05$, $\zeta_1 = 0.05$ and $\zeta_2 = 0.05$ are given for the coupled system, while frequency ratio α ranges from 0.1 to 10. Figure 4(a) shows that the peak magnitude of the total transmitted force FRF, $H_{f\ddot{x}_g}(\omega)$, is greater in the coupled system than in the uncoupled primary oscillator and is increased by increasing α. However, by considering individually the contribution through each oscillator, $H_{f_1\ddot{x}_g}(\omega)$ and $H_{f_2\ddot{x}_g}(\omega)$, a twofold effect becomes apparent: increments of α lead to a reduction in the peak transmitted force through the primary oscillator (Figure 4(b)) and, meanwhile, to an increase in the peak transmitted force through the secondary oscillator (Figure 4(c)). To quantify such variations in the transmitted force proportions, two ratios are defined in terms of FRF peak magnitude:

$$R_{f_1} = \frac{\max |H_{f_1\ddot{x}_g}(\omega)|^{\mathrm{C}}}{\max |H_{f_1\ddot{x}_g}(\omega)|^{\mathrm{U}}}, \qquad R_{f_2} = \frac{\max |H_{f_2\ddot{x}_g}(\omega)|^{\mathrm{C}}}{\max |H_{f_1\ddot{x}_g}(\omega)|^{\mathrm{U}}}, \tag{14}$$

where, as before, superscripts C and U denote the Coupled system and the Uncoupled primary oscillator, respectively. In Figures 5, R_{f_1} and R_{f_2} are plotted by varying mass ratio μ and frequency ratio α. Results indicate that, by selecting $\alpha > 1$, the rigid coupling to the secondary oscillator is able to reduce the peak transmitted force through the primary oscillator ($R_{f_1} < 1$) (Figures 5(a)). Such reductions increase by increasing α and μ and imply the simultaneous rise of the peak force through the secondary oscillator (Figures 5(b)).

4. Case study

Parametric analyses discussed in Section 3 indicate that the resonance response of a primary oscillator subjected to base motion can be reduced, as to relative displacement and internal forces, by way of the rigid coupling to a secondary oscillator, if the dynamic properties of the latter are purposely selected.

In this section, we deal with the seismic response of multi-degree-of-freedom frame structures and a case study is presented to explore how it could be affected by the rigid coupling to an exoskeleton structure.

4.1. Primary structure

A benchmark primary structure, located in a high seismicity site and not complying with the seismic performance requirements of current Italian Building Code [40], is considered. It consists of a 4-storey, 4 bays by 2 bays, reinforced concrete moment-resisting frame designed with non-ductile behaviour. Constant span length and inter-storey height are $l = 6\,\mathrm{m}$ and $h = 3.50\,\mathrm{m}$, respectively, with global dimensions of 24 m x 12 m x 14 m in the longitudinal (x), transverse (y) and vertical (z) directions. Distributions of mass and stiffness are uniform in plan and in elevation: columns and beams cross-sections are rectangular with dimensions 40x40 cm and 40x30 cm, respectively; total floor mass is equal to $238.42 \cdot 10^3$ kg. The structure is therefore symmetrical in plan with respect to both the x- and y-direction. A Finite Element (FE) model (Figure 6 (a)) has been developed by employing the OpenSees [41] module within the structural analysis program CDS WIN [42] . Floor slabs have been verified to have an in-plane rigid behaviour, entailing the introduction of a diaphragm constraint at each floor level.

4.2. Exoskeleton structure

A self-supporting exoskeleton structure, adjacent to the primary structure and provided with an independent foundation, is subsequently considered for retrofitting purposes (Figure 6 (b)). It consists of a diagrid-like structural system made of S235 steel columns and diagonal beams, whose cross-sections are HE100A and 114.3 mm x 5 mm circular hollow, respectively; the beam inclination angle is 49°. In the FE model of the coupled system, the exoskeleton structure is connected to the primary structure at each floor level by means of rigid links, preserving overall regularity in plan and in elevation.

4.3. Modal properties

Modal properties of the bare primary structure (i.e., in the absence of the exoskeleton structure) and of the coupled primary-exoskeleton system are reported in Table 1. In both cases, plans have two orthogonal axes of symmetry, the longitudinal x-axis and the transverse y-axis. Purely translational and perfectly uncoupled modes of vibration are therefore obtained, while rotational modes are evidenced by null participating mass ratios. The first two mode shapes of the bare primary structure and of the coupled primary-exoskeleton system are shown in Figure 7, together with the ones of the exoskeleton structure alone for completeness. Corresponding eigenvectors are normalised so to have the first component equal to unity.

Broadly speaking, natural frequencies of the coupled system are higher than the ones of the bare primary structure and this effect is more pronounced in the longitudinal x-direction than in the transverse y-direction. Considering the first two modes: the first natural frequency (corresponding to the first translational mode in transverse y-direction) increases by 86%, from 7.051 to 13.093 rad/s (period dropping from 0.891 to 0.480 s); the second natural frequency (corresponding to the first translational mode in longitudinal x-direction) increases by 129%, from 7.521 to 17.190 rad/s (period dropping from 0.835 to 0.366 s). It is worth observing that also the participating mass ratios vary between the bare primary structure and the coupled system. Specifically, they increase in the first two vibration modes and decrease in all the subsequent modes: for the first mode, M_y grows from 83.92% to 88.49%; for the second mode, M_x grows from 84.50% to 90.76%; for the subsequent modes, reductions of either M_y or M_x are obtained.

Based on the modal properties of primary structure and exoskeleton structure, it is possible to identify the nondimensional parameters that characterise the generalised model of the coupled system: mass ratio μ and frequency ratio α. Given the uncoupling of the dynamic response between the two horizontal directions, parameters are estimated independently in each direction: along x, μ is equal to 0.0087 and α is equal to 19.10; along y, μ is equal to 0.0085 and α

is equal to 13.50.

4.4. Seismic analyses

Response spectrum analyses are carried out on the FE models of the bare primary structure and of the coupled primary-exoskeleton system, with the aim of comparing their performance under earthquake loading. Seismic input is described by pseudo-acceleration response spectra according to the Italian Building Code [40]. A high seismicity site with soil class C (deposit of medium-dense sand) is considered and two seismic hazard levels are selected, defined in terms of a_g, the reference peak ground acceleration at bedrock: 1. $a_g = 0.082$g, with probability of exceedance of 63% in 50 years (mean return period 50 years), corresponding to the Damage Limitation (DL) performance requirement; 2. $a_g = 0.249$g, with probability of exceedance of 10% in 50 years (mean return period 475 years), corresponding to the Life Safety (LS) performance requirement. The relevant elastic pseudo-acceleration response spectra (5% viscous damping) are shown in Figure 8. Seismic action components are applied independently along each horizontal direction, x and y, evaluating separately the effects on the structural response [40, 43].

4.5. Seismic response

Monitored response quantities in seismic analyses are floor displacements relative to ground, inter-storey drifts, floor shear forces and floor pseudo-accelerations: from the viewpoint of seismic protection, they represent the engineering demand parameters which structural integrity and serviceability depend on.

Tables 2 and 3 report the peak floor displacements (U_x, U_y) and inter-storey drifts (Δ_x, Δ_y) obtained for the bare primary structure and for the coupled primary-exoskeleton system under the two considered levels of seismic excitation (DL and LS limit states). Variation of floor displacements over the height of the primary structure, both without and with the rigid coupling to the exoskeleton structure, is illustrated in Figure 9 for the LS limit state; in a similar way, Figure 10 depicts the profiles of inter-storey drift ratios for the DL state,

referring to an inter-story height of 3.50 m. In both Figures 9 and 10, the graphs on the left plot the peak response values, while a performance index (PI) is presented on the right, in order to comparatively assess the control performance at various elevations. Such PI is defined as the ratio of the peak floor response between the coupled primary-exoskeleton system and the bare primary structure: a value of PI smaller than one implies a reduced floor response in the coupled system as compared to the bare primary structure; conversely, a value greater than one means an amplification.

Due to the predominant contribution of the first vibration mode in both x- and y- direction, peak values of floor relative displacements grow along the height of the primary structure and this trend is found for the coupled primary-exoskeleton system as well (Figure 9 (a)). For the bare primary structure, peak floor displacements in the two horizontal directions are comparable, while for the coupled system, they are clearly smaller in the longitudinal (x) than in the transverse (y) direction: looking at PI (Figure 9 (b)), reductions range from 55% to 67% in x-direction and from 33% to 51% in y-direction, increasing with the increasing floor level; slightly lower reductions are obtained for the DL state, as reported in Table 2. These results are indicative of a differential performance in controlling the displacement response of the primary structure. The reason lies in the different dynamic properties exhibited by primary structure and exoskeleton structure in the two horizontal directions, and consequently, in the different nondimensional parameters characterising the coupled system. In particular, the higher value of frequency ratio α in x-direction is correlated with a more effective exoskeleton structure.

Peak inter-storey drift ratios for the bare primary structure are below 4‰, under DL state (Table 2), while they rise up to 10.5‰ and 11.2‰, corresponding to the second floor, under LS limit state (Table 3). For the coupled system, considerable reductions are observed, and particularly over the mid-storeys (second and third floor), where peak drifts are reduced by about 75% in x-direction and about 55% in y-direction, under both levels of seismic excitation. Profiles in Figure 10 show that a significant deformation control, although maximum at

mid-storeys, is achieved over the entire height of the primary structure.

In addition to displacement and deformation control, the rigid coupling to the exoskeleton structure leads to important reductions of the internal forces in the primary structure, both at the base and along the elevation. Tables 4 and 5 report the peak floor shear forces (V_x, V_y) obtained for the bare primary structure and for the coupled primary-exoskeleton system under DL and LS limit states.

Generally speaking, the rigid coupling to the exoskeleton structure may result in an increase of total base reactions, because of the added mass and of the reduction of vibration periods. However, due to the kinematic constraint, total base reactions on the coupled system are split among the primary structure and the exoskeleton structure. In particular, the base shear on the primary structure is found to be significantly reduced compared to its bare configuration. In Figure 11, the base shear on the primary structure is shown for both the horizontal directions and the two levels of seismic excitation: in x-direction, reductions amount to 38% under DL state and to 43% under LS limit state; in y-direction, reductions amount to 8% under DL state and to 17% under LS limit state. Greater reductions of base shear on the primary structure correspond, on the other hand, to higher values of base shear on the exoskeleton structure.

In Figure 12, profiles of peak floor shear forces along the height of the primary structure and of the exoskeleton structure are shown. Floor values are normalised by dividing by the corresponding base value on the bare primary structure. It is observed that shear forces on the primary structure are reduced at all floor levels, although the greatest reductions are found on the second and third floors, resulting in a significantly different distribution compared to the bare configuration. On the exoskeleton structure, shear forces are generally higher than on the primary structure.

According to theoretical investigations in Section 3, a trade-off is expected between deformation control and acceleration amplification. This result is confirmed by seismic analyses. Table 6 and 7 report the peak floor pseudo-accelerations (A_x, A_y) obtained for the bare primary structure and for the coupled primary-

exoskeleton system under the two levels of seismic excitation. Figure 13 illustrates their variation over the elevation for the LS limit state: peak values, normalised by gravity acceleration g, are depicted on the left, while corresponding PI is reported on the right. A general amplification of the acceleration response in the coupled system as compared to the bare primary structure is found, as indicated by values of PI greater than one: increments range from 28% to 95% in x-direction and from 38% to 89% in y-direction, decreasing with the increasing floor level; slightly higher increments are found for the DL state, as reported in Table 6. The amplification of floor accelerations appears to be a drawback in terms of vibration control, which should be carefully considered when acceleration-sensitive nonstructural components are involved in the retrofitting design.

5. Conclusions

This exploratory study was aimed at investigating whether exoskeleton structures can be a viable and effective means to control structural response under seismic loading. The exoskeleton structure is conceived as a dynamic system whose mass, stiffness and damping properties can be varied and, possibly, designed in order to modify the response of a primary structure, connected by way of a rigid coupling.

Frequency domain analyses have been used to characterise the dynamic behaviour of a coupled primary-secondary oscillator system and to discern the principle of operation delineated by the exoskeleton structure in terms of vibration control. The dynamic equilibrium of the coupled system has been set in non-dimensional form, to identify the governing independent parameters, and a parametric study has been carried out on the response to harmonic base motion. Ratios in terms of FRF peak magnitude have shown that the resonance response of the primary oscillator can be reduced, as to both displacements and internal forces, by virtue of the rigid coupling to the secondary oscillator, if the dynamic properties of the latter are purposely selected.

Seismic analyses have been subsequently conducted on a case study in which a mid-rise reinforced concrete frame structure, designed with non-ductile behaviour, is rigidly connected at each floor level to an exoskeleton structure, realised as a steel diagrid-like lattice structure. By comparing the seismic response of the bare primary structure and of the coupled primary-exoskeleton system, the following results emerge:

- a significant displacement and deformation control is achieved over the entire height of the primary structure: peak floor displacements are reduced, on average, by 40%–50%, while reductions of peak inter-storey drifts are higher and up to 75%;
- in addition to displacement and deformation control, important reductions of the internal forces in the primary structure are obtained, in terms of both base and floor shear forces; the need for strengthening the existing foundation below the primary structure is, consequently, avoided;
- greater reductions of the internal forces on the primary structure correspond, on the other hand, to higher internal forces on the exoskeleton structure;
- an amplification of the acceleration response is the expected trade-off for the achieved deformation control;
- a differential control performance is found between the two horizontal directions, due to the different dynamic properties exhibited by primary structure and exoskeleton structure in each direction.

The latter result suggests the possibility, worth being investigated, that an exoskeleton structure could be effective also in controlling the torsional response of unsymmetric-plan buildings. A multi-objective optimisation procedure, according to both performance and cost criteria, should be the subject of future research. The consideration of a dissipative exoskeleton structure, either showing nonlinear hysteretic behaviour or provided with supplemental damping devices, is of great interest and should be dealt with.

Acknowledgements

This research work was partially funded by the Italian Civil Protection Department under project RELUIS-DPC 2019-2021. Anna Reggio and Luciana Restuccia are also grateful to Politecnico di Torino for the financial support received in the form of a Starting Grant for Young Researchers (grants 57_ATEN_RSG16REGANN and 57_ATEN_RSG18RESLUC).

References

[1] A. Caverzan, M. Lamperti Tornaghi, P. Negro (Eds.), Proceedings of SAFESUST Workshop - A roadmap for the improvement of earthquake resistance and eco-efficiency of existing buildings and cities, Publications Office of the European Union, 2016. doi:10.2788/499080.

[2] A. Marini, C. Passoni, P. Riva, P. Negro, E. Romano, F. Taucer, Technology options for earthquake resistant, eco-efficient buildings in Europe: Research needs. EUR 26497 EN JRC87425, Technical Report, Publications Office of the European Union, 2014. doi:10.2788/68902.

[3] A. Belleri, A. Marini, Does seismic risk affect the environmental impact of existing buildings?, Energy and Buildings 110 (2016) 149–158.

[4] G. Housner, L. Bergman, T. Caughey, A. Chassiakos, R. Claus, S. F. Masri, R. E. Skelton, T. Soong, B. Spencer, J. Yao, Structural Control: Past, Present, and Future, Journal of Engineering Mechanics 123 (1997) 897–971.

[5] B. F. Spencer, S. Nagarajaiah, State of the Art of Structural Control, Journal of Structural Engineering 129 (2003) 845–856.

[6] M. Nakashima, O. Lavan, M. Kurata, Y. Luo, Earthquake engineering research needs in light of lessons learned from the 2011 Tohoku earthquake, Earthquake Engineering and Engineering Vibration 13 (2014) 141–149.

[7] T. E. Saaed, G. Nikolakopoulos, J.-E. Jonasson, H. Hedlund, A state-of-the-art review of structural control systems, Journal of Vibration and Control 21 (2015) 919–937.

[8] A. Reggio, L. Restuccia, G. A. Ferro, Feasibility and effectiveness of exoskeleton structures for seismic protection, Procedia Structural Integrity 9 (2018) 303–310.

[9] T. Trombetti, S. Silvestri, Novel schemes for inserting seismic dampers in shear-type systems based upon the mass proportional component of the Rayleigh damping matrix, Journal of Sound and Vibration 302 (2007) 486–526.

[10] O. Lavan, D. Abecassis, Seismic Behavior and Design of WallEDDFrame Systems, Frontiers in Built Environment 1 (2015) 1–17.

[11] R. Greco, G. C. Marano, Optimum design of viscous dissipative links in wall-frame systems, The Structural Design of Tall and Special Buildings 25 (2016) 412–428.

[12] Z. Qu, A. Wada, S. Motoyui, H. Sakata, S. Kishiki, Pin-supported walls for enhancing the seismic performance of building structures, Earthquake Engineering & Structural Dynamics 41 (2012) 2075–2091.

[13] N. Makris, M. Aghagholizadeh, The dynamics of an elastic structure coupled with a rocking wall, Earthquake Engineering & Structural Dynamics 46 (2017) 945–962.

[14] M. Aghagholizadeh, N. Makris, Earthquake response analysis of yielding structures coupled with vertically restrained rocking walls, Earthquake Engineering & Structural Dynamics 47 (2018) 2965–2984.

[15] A. Balducci, Dissipative Towers. Application n. EP2010074723820100831, WO2010EP62748 20100831, International and European classification E04H9/02; Italian concession n. 0001395591., 2005.

[16] N. Impollonia, A. Palmeri, Seismic performance of buildings retrofitted with nonlinear viscous dampers and adjacent reaction towers, Earthquake Engineering & Structural Dynamics 47 (2018) 1329–1351.

[17] L. Gioiella, E. Tubaldi, F. Gara, L. Dezi, A. Dall'Asta, Modal properties and seismic behaviour of buildings equipped with external dissipative pinned rocking braced frames, Engineering Structures 172 (2018) 807–819.

[18] L. Gioiella, E. Tubaldi, F. Gara, L. Dezi, A. Dall'Asta, Stochastic Seismic Analysis and Comparison of Alternative External Dissipative Systems, Shock and Vibration 2018 (2018) 1–16.

[19] L. Restuccia, T. Rosso, Smar-To: dalla riconnessione urbana all'esoscheletro intelligente. Proposta di riqualificazione urbana, energetica e strutturale di un edificio esistente (Supervisor: Prof. G.A. Ferro). Master's Thesis, Politecnico di Torino, 2012. URL: `http://opac.biblio.polito.it:80/F/?func=direct{&}doc{_}number=000338650{&}local{_}base=PTO01`.

[20] A. Marini, C. Passoni, A. Belleri, F. Feroldi, M. Preti, G. Metelli, P. Riva, E. Giuriani, G. Plizzari, Combining seismic retrofit with energy refurbishment for the sustainable renovation of RC buildings: a proof of concept, European Journal of Environmental and Civil Engineering 8189 (2017) 1–21.

[21] J. E. Luco, F. C. P. De Barros, Optimal damping between two adjacent elastic structures, Earthquake Engineering & Structural Dynamics Structural Dynamics 27 (1998) 649–659.

[22] E. Tubaldi, M. Barbato, A. Dall'Asta, Performance-based seismic risk assessment for buildings equipped with linear and nonlinear viscous dampers, Engineering Structures 78 (2014) 90–99.

[23] E. Tubaldi, Dynamic behavior of adjacent buildings connected by linear

viscous/viscoelastic dampers, Structural Control and Health Monitoring 22 (2015) 1086–1102.

[24] Y. L. Xu, Q. He, J. M. Ko, Dynamic response of damper-connected adjacent buildings under earthquake excitation, Engineering Structures 21 (1999) 135–148.

[25] T. Aida, T. Aso, K. Takeshita, T. Takiuchi, T. Fujii, Improvement of the structure damping performance by interconnection, Journal of Sound and Vibration 242 (2001) 333–353.

[26] J. Kim, J. Ryu, L. Chung, Seismic performance of structures connected by viscoelastic dampers, Engineering Structures 28 (2006) 183–195.

[27] V. Gattulli, F. Potenza, M. Lepidi, Damping performance of two simple oscillators coupled by a visco-elastic connection, Journal of Sound and Vibration 332 (2013) 6934–6948.

[28] Y. Q. Ni, J. M. Ko, Z. G. Ying, Random seismic response analysis of adjacent buildings coupled with non-linear hysteretic dampers, Journal of Sound and Vibration 246 (2001) 403–417.

[29] A. V. Bhaskararao, R. S. Jangid, Seismic analysis of structures connected with friction dampers, Engineering Structures 28 (2006) 690–703.

[30] M. Basili, M. De Angelis, Optimal passive control of adjacent structures interconnected with nonlinear hysteretic devices, Journal of Sound and Vibration 301 (2007) 106–125.

[31] S. D. Bharti, S. M. Dumne, M. K. Shrimali, Seismic response analysis of adjacent buildings connected with MR dampers, Engineering Structures 32 (2010) 2122–2133.

[32] K. S. Park, S. Y. Ok, Optimal design of actively controlled adjacent structures for balancing the mutually conflicting objectives in design preference aspects, Engineering Structures 45 (2012) 213–222.

[33] V. Gattulli, F. Potenza, B. F. Spencer, Design criteria for dissipative devices in coupled oscillators under seismic excitation, Structural Control and Health Monitoring 25 (2018) e2167.

[34] V. Tomei, M. Imbimbo, E. Mele, Optimization of structural patterns for tall buildings: The case of diagrid, Engineering Structures 171 (2018) 280–297.

[35] S. Labò, C. Passoni, A. Marini, A. Belleri, G. Camata, P. Riva, E. Spacone, Prefabricated responsive diagrid for holistic renovation of existing mid-rise RC buildings, in: Proceedings of COMPDYN 2017 - 6th ECCOMAS Thematic Conference on Computational Methods in Structural Dynamics and Earthquake Engineering, Rhode Island, Greece, 2017, pp. June 15–17. doi:10.7712/120117.

[36] B. F. Spencer, J. Suhardjo, M. Sain, Frequency domain optimal control strategies for aseismic protection, Journal of Engineering Mechanics ASCE 120 (1994) 135–158.

[37] C. M. Harris, A. G. Piersol, T. L. Paez, Harris' Shock and Vibration Handbook, 6th ed., McGraw-Hill, New York, USA, 2010.

[38] G. Genta, Vibration Dynamics and Control, Springer, 2009.

[39] D. Inman, Engineering Vibration, 4th ed., Pearson Prentice Hall, Upper Saddle River, NJ, USA, 2014.

[40] Ministero delle Infrastrutture e dei Trasporti, Norme Tecniche per le Costruzioni, D.M. 17.01.2018, Rome, 2018.

[41] F. McKenna, G. Fenves, M. Scott, B. Jeremic, Open system for earthquake engineering simulation (OpenSees), version 2.4.6, Pacific Earthquake Engineering Research Center, University of California at Berkeley, USA, 2013.

[42] STS, CDS Win Documentation, www.stsweb.it, 2018.

[43] European Committee for Standardization (CEN), Eurocode 8: Design of structures for earthquake resistance Part. 1: General rules, seismic actions and rules for buildings, EN 1998-1., Brussels, 2004.

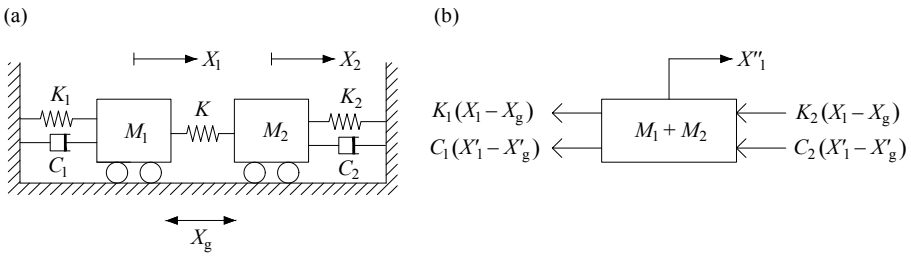

Figure 1: Coupled primary-secondary oscillator system: (a) structural model; (b) free body diagram in case of rigid coupling ($K \to \infty$).

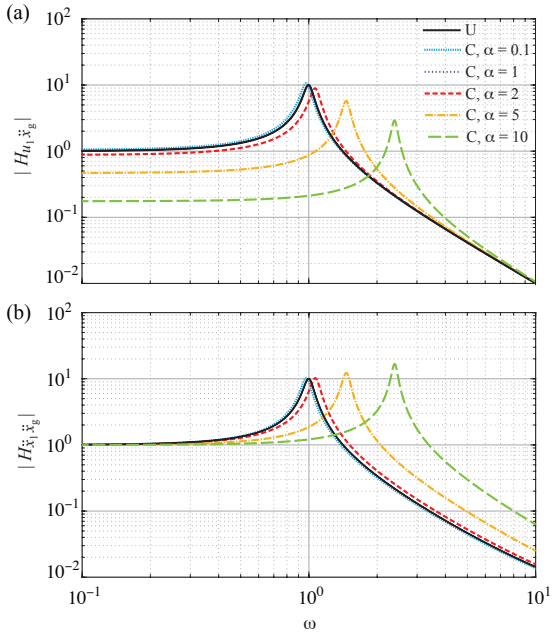

Figure 2: Magnitude of the FRFs (a) $H_{u_1\ddot{x}_g}$ of relative displacement and (b) $H_{\ddot{x}_1\ddot{x}_g}$ of absolute acceleration, for the Uncoupled (U) primary oscillator and for the Coupled (C) system with varying frequency ratio α. It is assumed $\mu = 0.05$, $\zeta_1 = 0.05$ and $\zeta_2 = 0.05$.

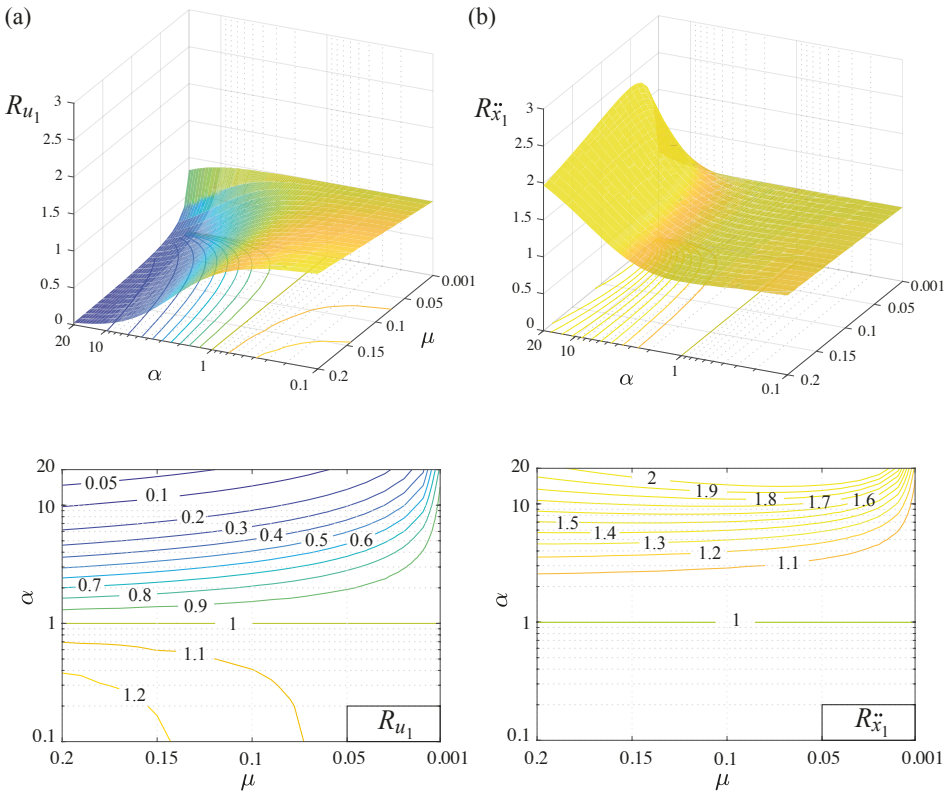

Figure 3: Surface and contour plots of response ratios (a) R_{u_1} for relative displacement and (b) $R_{\ddot{x}_1}$ for absolute acceleration, versus mass ratio μ and frequency ratio α. It is assumed $\zeta_1 = 0.05$ and $\zeta_2 = 0.05$.

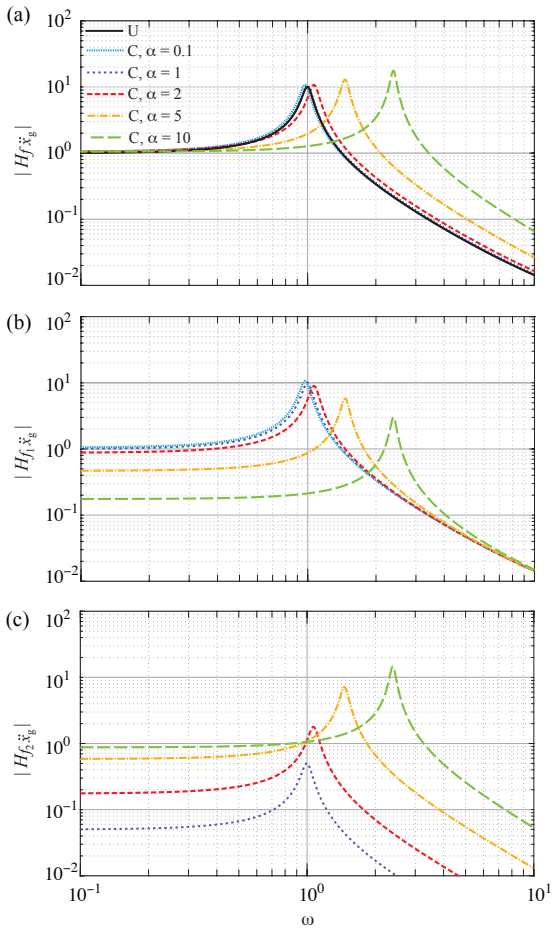

Figure 4: Magnitude of the FRFs (a) $H_{f\ddot{x}_g}$ of total transmitted force, (b) $H_{f_1\ddot{x}_g}$ of force transmitted through primary oscillator and (c) $H_{f_2\ddot{x}_g}$ of force transmitted through secondary oscillator, for the Uncoupled (U) primary oscillator and for the Coupled (C) system with varying frequency ratio α. It is assumed $\mu = 0.05$, $\zeta_1 = 0.05$ and $\zeta_2 = 0.05$.

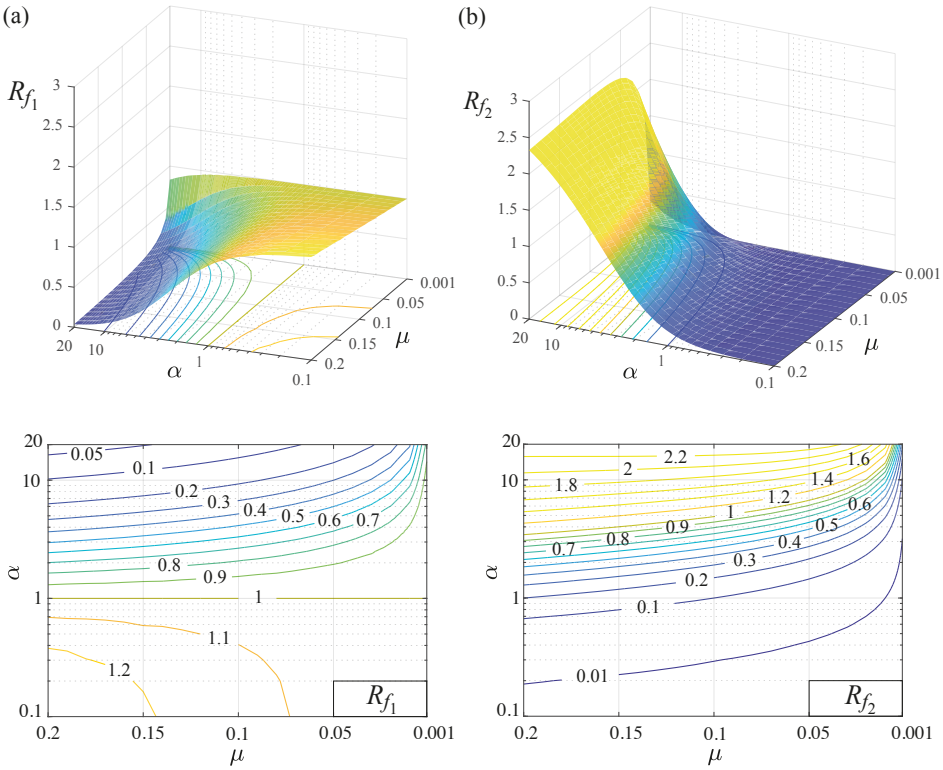

Figure 5: Surface and contour plots of transmitted force ratios (a) R_{f_1} for the force through the primary oscillator and (b) R_{f_2} for the force through the secondary oscillator, versus mass ratio μ and frequency ratio α. It is assumed $\zeta_1 = 0.05$ and $\zeta_2 = 0.05$.

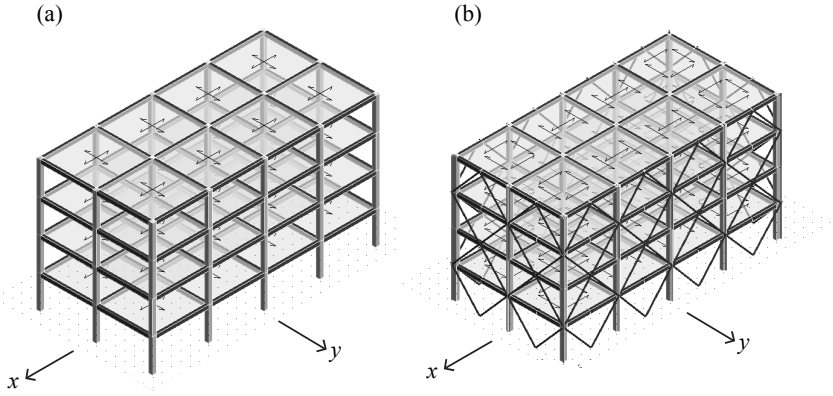

Figure 6: Three-dimensional views of the FE models of (a) bare primary structure and of (b) coupled primary-exoskeleton system.

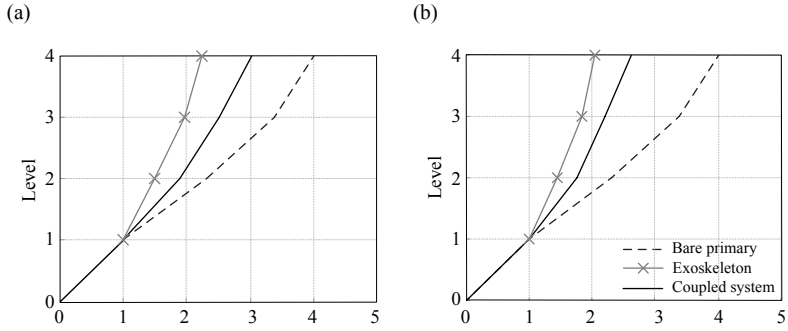

Figure 7: Mode shapes of bare primary structure, exoskeleton structure and coupled primary-exoskeleton system: (a) first mode (translational in y-direction); second mode (translational in x-direction).

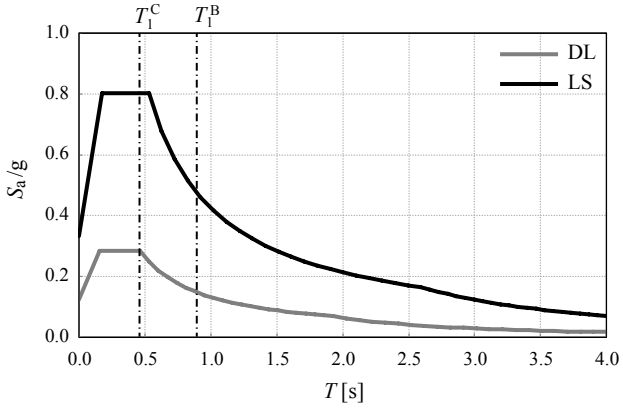

Figure 8: Elastic pseudo-acceleration response spectra (5% viscous damping) defined for the Damage Limitation (DL) and Life Safety (LS) performance requirements, according to the Italian Building Code [40]. Dash-dot lines indicate the fundamental vibration period of the Bare primary structure ($T_1^{\mathrm{B}} = 0.891\,\mathrm{s}$) and of the Coupled primary-exoskeleton system ($T_1^{\mathrm{C}} = 0.480\,\mathrm{s}$).

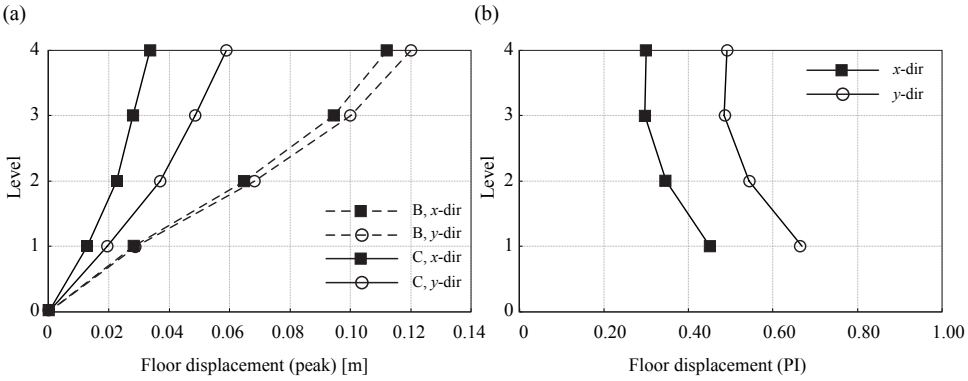

Figure 9: Profiles of floor displacements in x- and y-direction: (a) peak values for the Bare primary structure (B) and for the Coupled primary-exoskeleton system (C); (b) Performance Index (PI). Life Safety limit state.

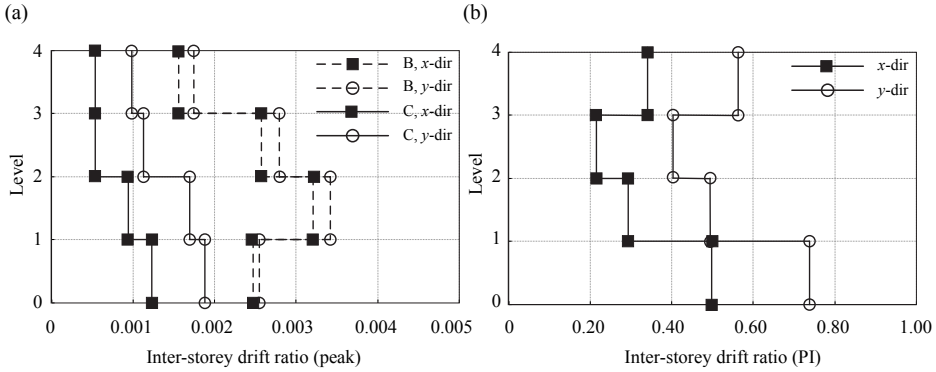

Figure 10: Profiles of inter-storey drift ratios in x- and y-direction: a) peak values for the Bare primary structure (B) and for the Coupled primary-exoskeleton system (C); (b) Performance Indices (PI). Damage Limitation state.

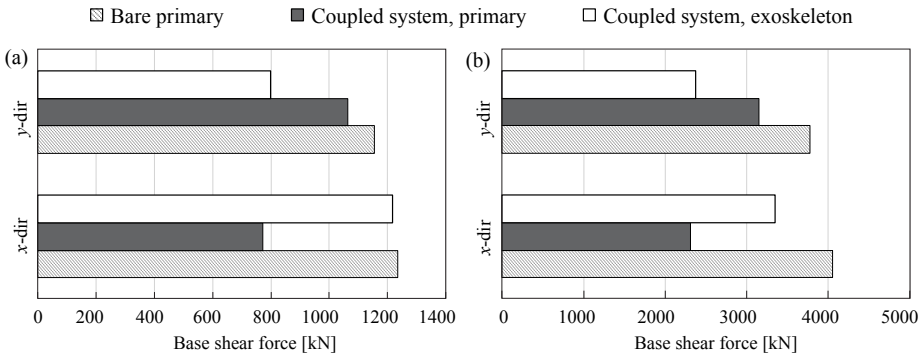

Figure 11: Peak base shear forces at (a) Damage Limitation state and (b) Life Safety limit state: comparison between bare primary structure and coupled primary-exoskeleton system.

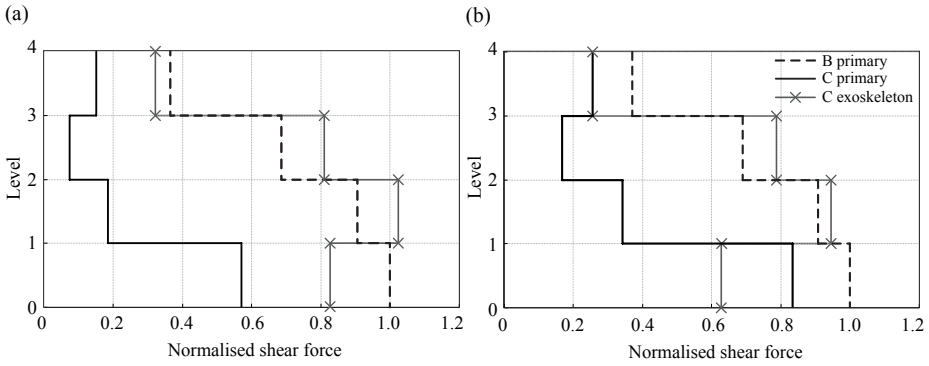

Figure 12: Profiles of normalised peak floor shear forces in (a) x- and (b) y-direction: comparison between Bare (B) primary structure and Coupled (C) primary-exoskeleton system. Life Safety limit state.

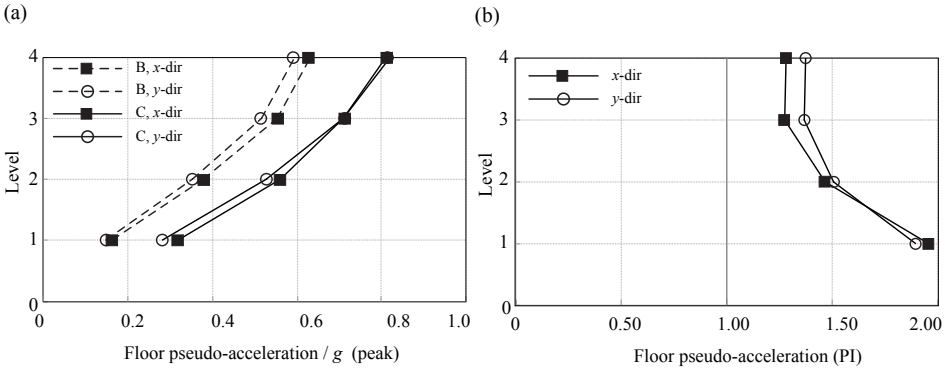

Figure 13: Profiles of floor pseudo-accelerations in x- and y-direction: (a) peak values, normlised by g, for the Bare primary structure (B) and for the Coupled primary-exoskeleton system (C); (b) Performance Index (PI). Life Safety limit state.

496

TABLES

	Bare primary structure				Coupled primary-exoskeleton system			
	Ω	T	M_x	M_y	Ω	T	M_x	M_y
Mode	[rad/s]	[s]	[%]	[%]	[rad/s]	[s]	[%]	[%]
1	7.051	0.891	0.00	83.92	13.093	0.480	0.00	88.49
2	7.521	0.835	84.53	0.00	17.190	0.366	90.76	0.00
3	8.226	0.764	0.00	0.00	22.345	0.281	0.00	0.00
4	23.372	0.269	0.00	11.04	36.639	0.171	0.00	7.71
5	24.520	0.256	10.73	0.00	45.858	0.137	5.96	0.00
6	26.879	0.234	0.00	0.00	58.214	0.108	0.00	0.00
7	44.571	0.141	0.00	3.94	68.354	0.092	0.00	2.80
8	45.789	0.137	3.74	0.00	82.744	0.076	2.44	0.00
9	50.643	0.124	0.00	0.00	87.110	0.072	0.00	1.00
10	67.630	0.093	0.00	1.10	97.434	0.064	0.84	0.00
11	68.192	0.092	1.01	0.00	103.530	0.061	0.00	0.00
12	76.243	0.082	0.00	0.00	119.519	0.053	0.00	0.00

Table 1: Modal properties of the bare primary structure and of the coupled primary-exoskeleton system: circular frequencies Ω, periods T, participating mass ratios M_x and M_y in x- and y-direction, respectively.

	Bare primary structure				Coupled primary-exoskeleton system			
	U_x	U_y	Δ_x	Δ_y	U_x	U_y	Δ_x	Δ_y
Level	[m]	[m]	[‰]	[‰]	[m]	[m]	[‰]	[‰]
1	0.009	0.009	2.5	2.5	0.004	0.007	1.2	1.9
2	0.020	0.021	3.2	3.4	0.008	0.013	0.9	1.7
3	0.029	0.031	2.6	2.8	0.009	0.016	0.5	1.1
4	0.034	0.037	1.6	1.7	0.011	0.020	0.5	1.0

Table 2: Peak floor displacements (U_x, U_y) and inter-storey drift ratios (Δ_x, Δ_y) in x- and y-direction for the bare primary structure and for the coupled primary-exoskeleton system, Damage Limitation state.

	Bare primary structure				Coupled primary-exoskeleton system			
	U_x	U_y	Δ_x	Δ_y	U_x	U_y	Δ_x	Δ_y
Level	[m]	[m]	[‰]	[‰]	[m]	[m]	[‰]	[‰]
1	0.028	0.029	8.1	8.3	0.013	0.019	3.6	5.6
2	0.065	0.068	10.5	11.2	0.023	0.037	2.8	5.0
3	0.094	0.100	8.4	9.1	0.028	0.049	1.6	3.3
4	0.112	0.120	5.1	5.7	0.034	0.059	1.6	3.0

Table 3: Peak floor displacements (U_x, U_y) and inter-storey drift ratios (Δ_x, Δ_y) in x- and y-direction for the bare primary structure and for the coupled primary-exoskeleton system, Life Safety limit state.

	Bare primary structure		Coupled primary-exoskeleton system			
	V_x	V_y	$V_{x,\,\mathrm{prim}}$	$V_{x,\,\mathrm{exo}}$	$V_{y,\,\mathrm{prim}}$	$V_{y,\,\mathrm{exo}}$
Level	[kN]	[kN]	[kN]	[kN]	[kN]	[kN]
1	1236	1154	771	1218	1063	799
2	1118	1048	253	1470	434	1204
3	846	797	104	1155	207	1010
4	453	426	212	460	326	327

Table 4: Peak floor shear forces (V_x, V_y) in x- and y-direction for the bare primary structure and for the coupled primary-exoskeleton system, Damage Limitation state.

	Bare primary structure		Coupled primary-exoskeleton system			
	V_x	V_y	$V_{x,\,\mathrm{prim}}$	$V_{x,\,\mathrm{exo}}$	$V_{y,\,\mathrm{prim}}$	$V_{y,\,\mathrm{exo}}$
Level	[kN]	[kN]	[kN]	[kN]	[kN]	[kN]
1	4053	3773	2311	3347	3146	2371
2	3669	3426	749	4152	1287	3567
3	2779	2605	299	3283	634	2972
4	1481	1394	612	1299	966	968

Table 5: Peak floor shear forces (V_x, V_y) in x- and y-direction for the bare primary structure and for the coupled primary-exoskeleton system, Life Safety limit state.

	Bare primary structure		Coupled primary-exoskeleton system	
	A_x	A_y	A_x	A_y
Level	[m/s^2]	[m/s^2]	[m/s^2]	[m/s^2]
1	0.493	0.445	1.107	0.931
2	1.142	1.054	1.928	1.752
3	1.666	1.554	2.445	2.349
4	1.900	1.788	2.793	2.716

Table 6: Peak floor pseudo-accelerations (A_x, A_y) in x- and y-direction for the bare primary structure and for the coupled primary-exoskeleton system, Damage Limitation state.

	Bare primary structure		Coupled primary-exoskeleton system	
	A_x	A_y	A_x	A_y
Level	[m/s^2]	[m/s^2]	[m/s^2]	[m/s^2]
1	1.611	1.456	3.149	2.759
2	3.733	3.445	5.485	5.189
3	5.445	5.079	6.956	6.957
4	6.212	5.846	7.947	8.044

Table 7: Peak floor pseudo-accelerations (A_x, A_y) in x- and y-direction for the bare primary structure and for the coupled primary-exoskeleton system, Life Safety limit state.